



Accepted Article

Title: Exerting Spatial Control During Nanoparticle Occlusion within Calcite Crystals

Authors: Yin Ning, Yide Han, Lijuan Han, Matthew J. Derry, and Steven P. Armes

This manuscript has been accepted after peer review and appears as an Accepted Article online prior to editing, proofing, and formal publication of the final Version of Record (VoR). This work is currently citable by using the Digital Object Identifier (DOI) given below. The VoR will be published online in Early View as soon as possible and may be different to this Accepted Article as a result of editing. Readers should obtain the VoR from the journal website shown below when it is published to ensure accuracy of information. The authors are responsible for the content of this Accepted Article.

To be cited as: *Angew. Chem. Int. Ed.* 10.1002/anie.202007110

Link to VoR: <https://doi.org/10.1002/anie.202007110>

Exerting Spatial Control During Nanoparticle Occlusion within Calcite Crystals

Yin Ning,^{*[a]} Yide Han,^[a] Lijuan Han,^[a] Matthew J. Derry,^{[a],[b]} and Steven P. Armes^{*[a]}

[a] Dr. Y. Ning, Y. Han, L. Han, Dr. M. J. Derry and Prof. S. P. Armes
Department of Chemistry, University of Sheffield, Brook Hill, Sheffield, South Yorkshire S3 7HF, U.K.
E-mail: ningyin925@126.com; s.p.arnes@sheffield.ac.uk

[b] Dr. M. J. Derry
Present address: Aston Institute of Materials Research, Aston University, Birmingham, B4 7ET, U.K.

Supporting information for this article is given via a link at the end of the document.

Abstract: In principle, nanoparticle occlusion within crystals provides a straightforward and efficient route to make new nanocomposite materials. However, developing a deeper understanding of the design rules underpinning this strategy is highly desirable. In particular, controlling the spatial distribution of the guest nanoparticles within the host crystalline matrix remains a formidable challenge. Herein, we show that the surface chemistry of the guest nanoparticles and the $[Ca^{2+}]$ concentration play critical roles in determining the precise *spatial* location of the nanoparticles within calcite crystals. Moreover, *in situ* studies provide important mechanistic insights regarding *surface-confined* nanoparticle occlusion. Overall, this study not only provides useful guidelines for efficient nanoparticle occlusion, but also enables the rational design of patterned calcite crystals using model anionic block copolymer vesicles.

Introduction

At first sight, nanoparticle occlusion within inorganic crystals appears to be highly counter-intuitive because crystallization is normally considered to involve expulsion of impurities, rather than their incorporation. Nevertheless, efficient nanoparticle occlusion can occur under optimized conditions,^[1] producing nanocomposite crystals that differ significantly from those hybrid materials produced via conventional chemical or mechanical mixing.^[2] In some cases, such nanocomposite crystals can exhibit enhanced hardness and toughness compared to their geological counterparts.^[3] Clearly, intimate interaction between the guest nanoparticles and the growing host crystals is a prerequisite for efficient nanoparticle occlusion.^[4] Thus the nanoparticles must possess appropriate surface chemistry and optimization of the steric stabilizer type, chain length, charge density and surface density may be required to achieve maximum occlusion efficiency under a given set of crystal growth conditions.^[5] Much current research has focused on the design of model guest nanoparticles, rather than systematic variation of the crystal growth parameters (e.g. metal cation concentration, rate of crystal growth, pH, temperature etc.) that affect nanoparticle occlusion. In particular, the effect of simultaneously optimizing the nanoparticle surface chemistry and the crystal growth conditions on nanoparticle occlusion has not yet been studied. In addition, it remains technically challenging to exert spatial control during nanoparticle occlusion within host crystals.

Over the past decade, polymerization-induced self-assembly (PISA) has become widely recognized as a powerful platform technology for the rational design of a wide range of block copolymer nano-objects.^[6] Using robust techniques such as reversible addition-fragmentation chain transfer (RAFT) polymerization^[7] to perform PISA syntheses ensures that a wide range of functional monomers can be utilized^[8] and enables the preparation of sterically-stabilized nanoparticles at high copolymer concentrations.^[9]

Herein a series of anionic poly(methacrylic acid)_x-poly(benzyl methacrylate)₂₀₀ (PMAA_x-PBzMA₂₀₀) diblock copolymer vesicles is prepared via PISA while varying the mean degree of polymerization (DP, or *x*) of the PMAA stabilizer block. Calcite crystals are then precipitated in the presence of such vesicles while systematically varying the calcium ion concentration. The aim of such experiments is to examine the combined effect of PMAA DP and $[Ca^{2+}]$ on nanoparticle occlusion within calcite single crystals. *In situ* studies provide further important insights that enable exquisite control to be exerted over the precise spatial location of the vesicles incorporated within the host matrix. These new findings enabled the construction of patterned vesicle/calcite nanocomposite crystals using a multi-step nanoparticle occlusion strategy.

Results and Discussion

Synthesis and Characterization of Diblock Copolymer Vesicles Prepared via RAFT-mediated PISA. First, a series of poly(methacrylic acid)_x (PMAA_x) homopolymers with varying mean DPs (*x* = 28, 35, 54 or 72) was prepared by RAFT solution polymerization of MAA in ethanol (**Table S1**, detailed synthesis protocols are provided in Supplementary Information). Such precursors were then chain-extended via RAFT dispersion polymerization of benzyl methacrylate in various alcoholic media targeting a mean DP of 200 in each case (**Figure 1a** and **Table S2**). Adjusting the solvent composition enables near-monodisperse PMAA-PBzMA vesicles to be obtained. For example, using a methanol-rich methanol/ethanol mixture leads to relatively uniform vesicles when using a PMAA DP of 28. A small amount (0.5 mol%) of fluorescein *O*-methacrylate was copolymerized with BzMA to produce vesicles with fluorescently-labeled membranes (**Figure 1a**). This facilitates visualization of the vesicles within the calcite crystals by confocal laser scanning microscopy (CLSM). These model vesicles were transferred into

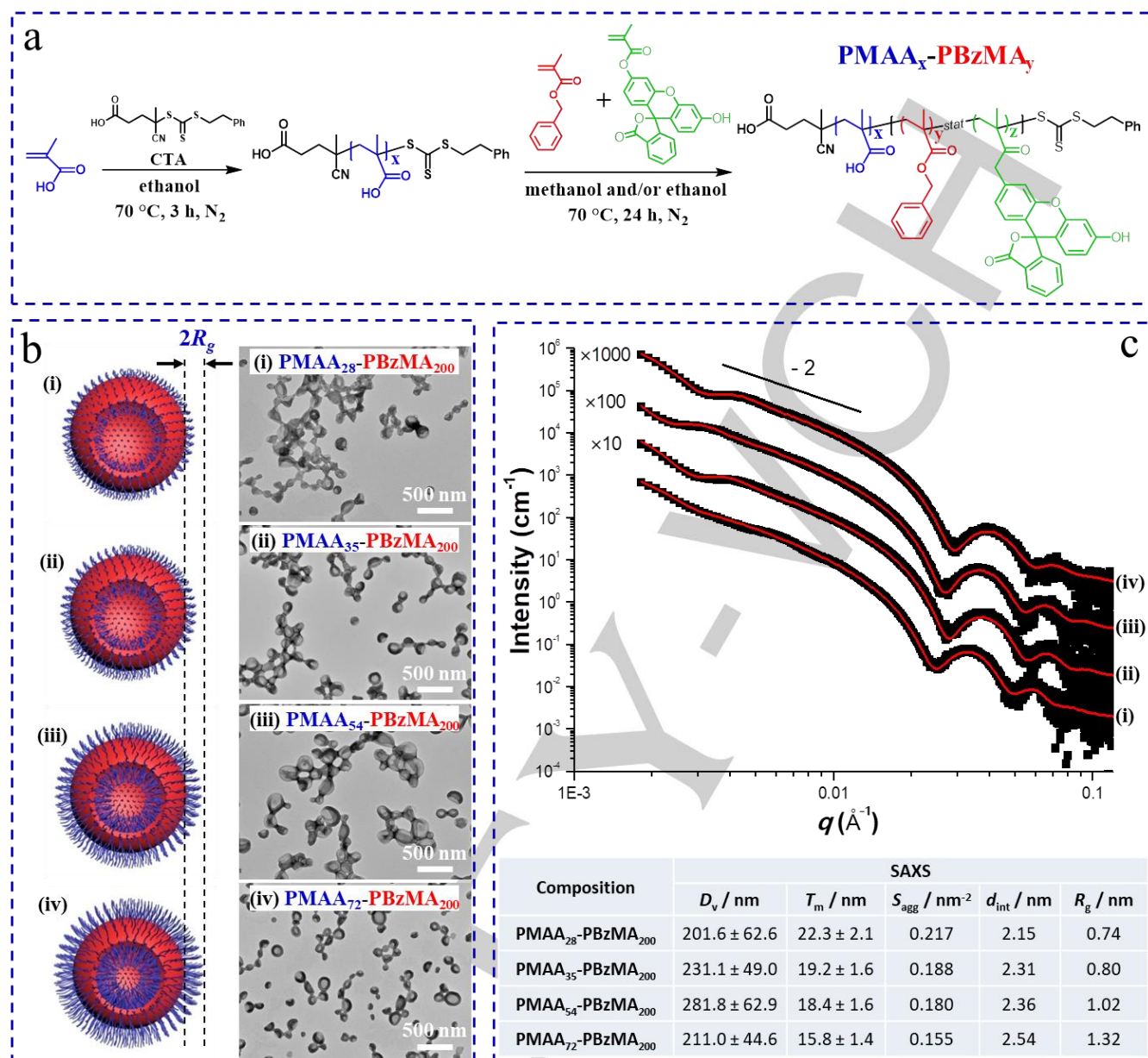


Figure 1. Synthesis and characterization of diblock copolymer model vesicles. (a) PISA synthesis of poly(methacrylic acid)_x-poly(benzyl methacrylate)_y (PMAA_x-PBzMA_y) diblock copolymer vesicles via RAFT alcoholic dispersion polymerization; (b) schematic cartoon and corresponding transmission electron micrograph for each type of vesicle, illustrating the thicker steric stabilizer layer with increasing x and the well-defined vesicular morphology. (c) SAXS patterns (black) and corresponding data fits (red) recorded for 1.0% w/w aqueous dispersions of PMAA₂₈-PBzMA₂₀₀ vesicles, PMAA₃₅-PBzMA₂₀₀ vesicles, PMAA₅₄-PBzMA₂₀₀ vesicles, and PMAA₇₂-PBzMA₂₀₀ vesicles. The corresponding table summarizes the structure parameters derived from the data fits using a well-known scattering model for vesicles.^[10] D_v = volume-average diameter; T_m = mean membrane thickness; S_{agg} = number of copolymer chains per unit surface area; d_{int} = mean distance between adjacent chains at the core-shell interface and R_g = radius of gyration. The vesicle aggregation observed in the TEM images of Figure 1b is just a drying artefact.^[11]

aqueous media by centrifugation (five cycles at 10,000 rpm for 30 min) with each supernatant being carefully decanted and replace with deionized water. This transfer leads to ionization of the acidic PMAA chains, which acquire substantial anionic character.^[5b] Varying the mean DP of the PMAA chains enables the steric stabilizer layer thickness ($2R_g$) to be adjusted (Figure 1b). Gel permeation chromatography (GPC) analysis indicated that the PMAA_x homopolymers and the corresponding PMAA_x-PBzMA₂₀₀ diblock copolymers exhibit relatively narrow molecular weight distributions, indicating well-controlled RAFT

polymerizations and high blocking efficiencies (Figure S1). Electron microscopy studies confirmed that relatively uniform vesicles were formed by each of the four PMAA_x-PBzMA₂₀₀ diblock copolymers (Figure 1b and Figure S2).

Small-angle X-ray scattering (SAXS) studies were performed to further characterize these four model vesicles. Each SAXS pattern exhibited a low q gradient of -2, indicating a vesicular morphology that is in good agreement with transmission electron microscopy (TEM) studies (see Figures 1b and c).^[12] Perhaps more importantly, satisfactory data fits to all four SAXS patterns

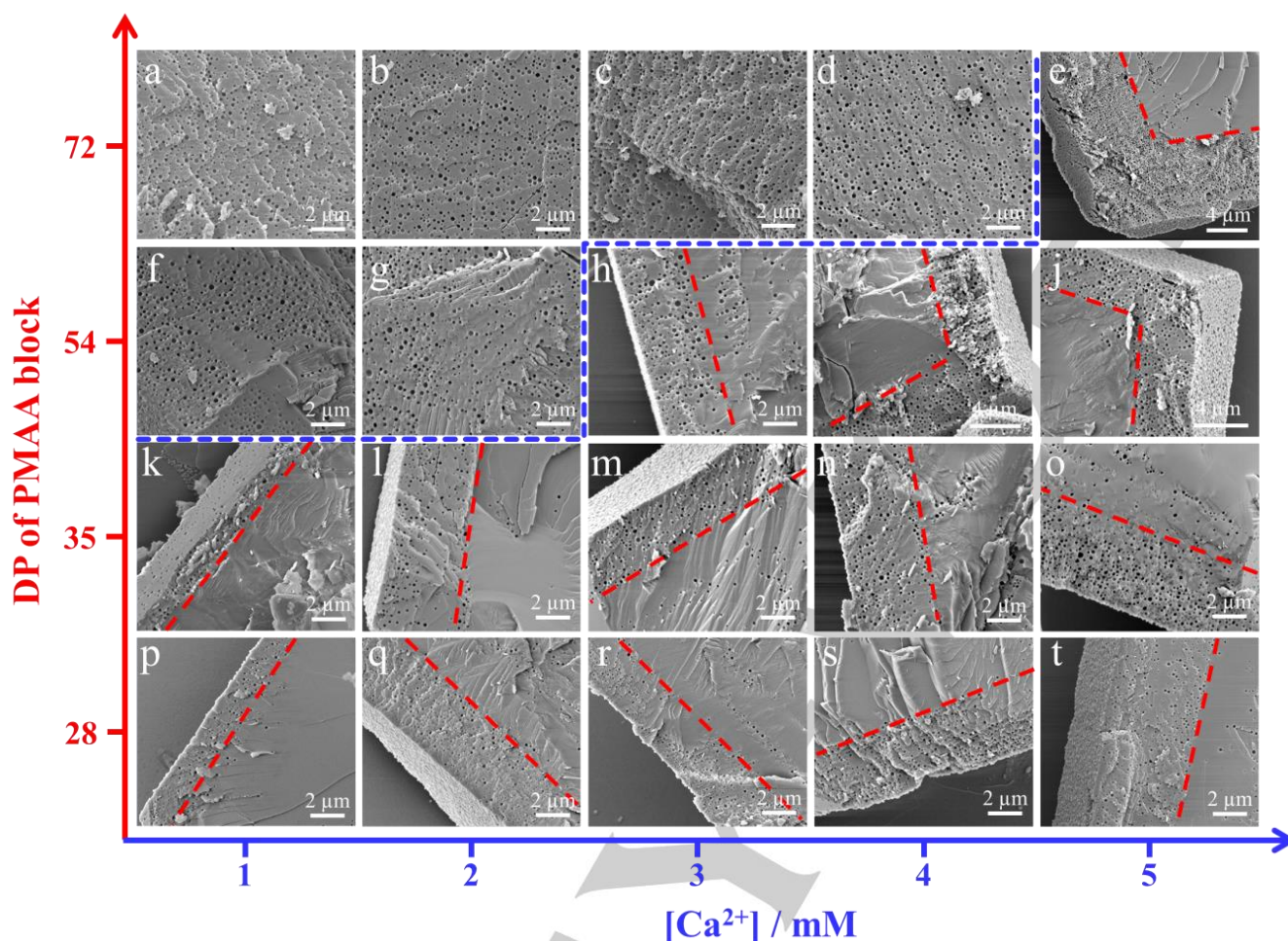


Figure 2. SEM images recorded for randomly-fractured calcite crystals precipitated in the presence of $[\text{Ca}^{2+}]$ concentrations ranging from 1 mM to 5 mM and PMAA_x-PBzMA₂₀₀ vesicles where $x = 28, 35, 54$ or 72. Red dashed lines depict the boundary between occlusion and no occlusion. Dense *uniform* occlusion of vesicles is observed within crystals shown above the blue dashed line, whereas crystals shown below this boundary exhibit only *surface-confined* occlusion.

can be achieved using a well-known scattering model developed for vesicles.^[10] The overall volume-average vesicle diameter varies from ~200 nm to ~280 nm, which is much bigger than the corresponding spheres and thus facilitates their visualization via scanning electron microscopy (SEM).^[11] Given that the target PBzMA DP for these vesicles was held constant at 200, it is interesting that somewhat thinner vesicle membranes are formed as the DP of the PMAA stabilizer is increased from 28 to 72 (see Table in **Figure 1c**). Moreover, the number of copolymer chains per unit area (S_{agg}) is also reduced, so the mean inter-chain separation distance at the stabilizer/membrane interface (d_{int}) is accordingly increased. These observations suggest that longer stabilizer chains lead to greater interdigitation of the PBzMA chains within the membrane.^[13] As expected, increasing the PMAA DP led to a thicker steric stabilizer layer ($2R_g$), ranging from 1.48 nm to 2.64 nm (see tabulated data provided in **Figure 1c**).

Combined Effect of the Systematic Variation of the PMAA Stabilizer DP and $[\text{Ca}^{2+}]$ on Nanoparticle Occlusion. Calcium carbonate (CaCO_3) crystals were precipitated using the well-known ammonia diffusion method.^[14] Calcite was selected as a host crystal because it is an abundant natural mineral, forms relatively large single crystals and is considered to be

environmentally benign. To establish an appropriate $[\text{Ca}^{2+}]$ for the production of pure calcite, control experiments were conducted over a range of $[\text{Ca}^{2+}]$ in the absence of any additives. Well-defined rhombohedral crystals were obtained for $[\text{Ca}^{2+}] = 1\text{--}20$ mM. However, mixed phases were observed for higher $[\text{Ca}^{2+}]$ (**Figure S3**). Hence, $[\text{Ca}^{2+}] \sim 1\text{--}5$ mM were selected for the preparation of calcium carbonate crystals in the presence of 0.05% w/w PMAA_x-PBzMA₂₀₀ vesicles. Raman spectroscopy studies confirmed that the rhombohedral crystals were indeed calcite (**Figure S4**). Interestingly, dense, uniform occlusion was achieved for PMAA₇₂-PBzMA₂₀₀ vesicles for $[\text{Ca}^{2+}] = 1\text{--}4$ mM (see **Figures 2a-d**). However, at $[\text{Ca}^{2+}] = 5$ mM, vesicles were mainly incorporated at the near-surface region (~5 μm) of the crystal (see **Figure 2e**). Such *surface-confined* occlusion was also observed when the $[\text{Ca}^{2+}]$ was increased up to 20 mM (**Figure S5**). Moreover, control experiments confirmed that only *surface-confined* occlusion occurred when varying the vesicle concentration from 0.005 to 0.10% w/w (see **Figure S6**). However, denser - but still *surface-confined* - occlusion was observed at higher vesicle concentrations (**Figures S6e-h**). This suggests that *surface-confined* occlusion is not the result of vesicle concentration. We then examined PMAA₅₄-PBzMA₂₀₀ vesicles under identical conditions and found that

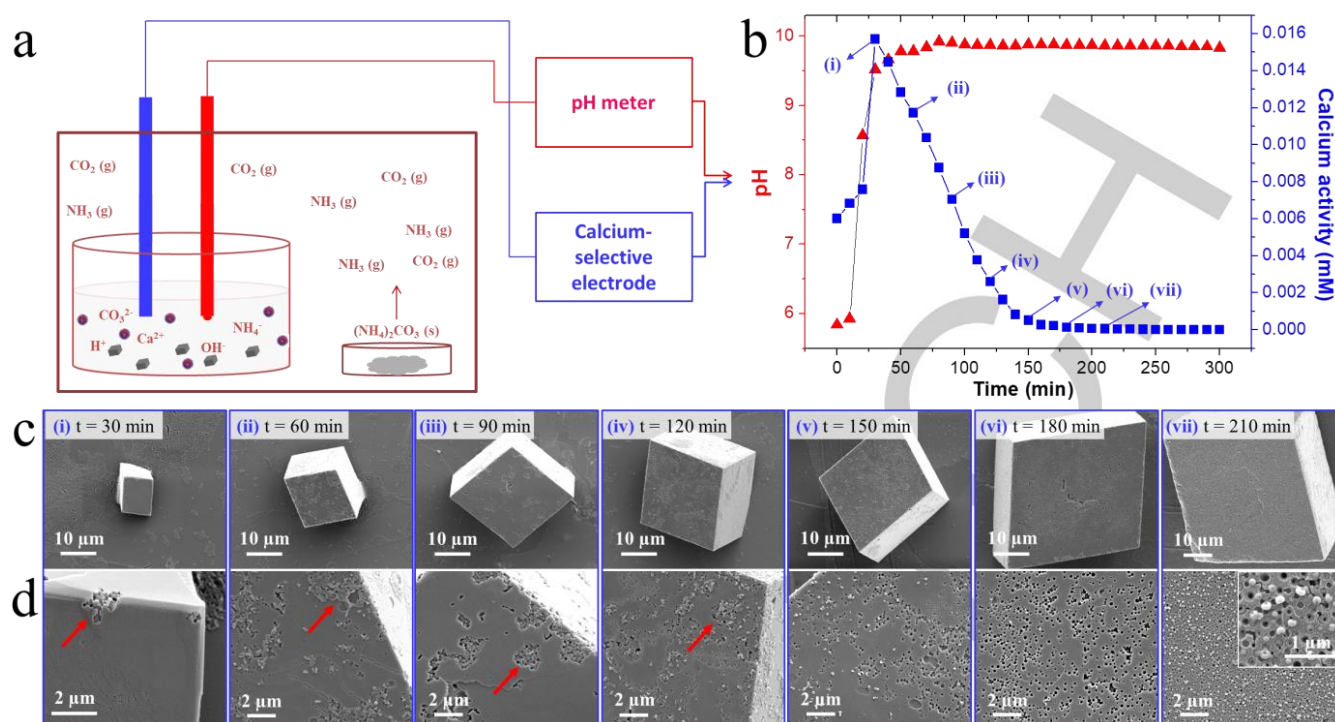


Figure 3. *In situ* monitoring of the solution pH and calcium activity during formation of calcite crystals in the presence of 0.05% w/w PMAA₇₂-PBzMA₂₀₀ vesicles at an initial $[Ca^{2+}]$ of 10 mM. (a) Schematic diagram for the experimental set-up; (b) evolution in solution pH and calcium activity over time; (c) SEM images recorded for growing crystals periodically taken from the reaction solution at different time points; (d) higher magnification SEM images of the corresponding samples shown in (c). Further SEM images are provided in the supplementary information (Figure S8).

surface-confined occlusion only occurred for $[Ca^{2+}] \geq 3$ mM (Figures 2f-j). Finally, using PMAA₃₅-PBzMA₂₀₀ and PMAA₂₈-PBzMA₂₀₀ vesicles always resulted in *surface-confined* occlusion even at $[Ca^{2+}] = 1$ mM (Figures 2k-t). These observations suggest that both the PMAA DP and the $[Ca^{2+}]$ can influence whether *uniform* occlusion or *surface-confined* occlusion occurs. In summary, a relatively high PMAA DP and low $[Ca^{2+}]$ favour *uniform* occlusion (see top-left region in Figure 2) while shorter PMAA chains and high $[Ca^{2+}]$ result in *surface-confined* occlusion (see bottom-right region in Figure 2).

In Situ Monitoring During Surface-confined Occlusion of Anionic Vesicles. How can we account for the above experimental observations? *Surface-confined* occlusion suggests that the vesicles are only incorporated within the calcite host during the latter stages of crystallization, where the $[Ca^{2+}]$ is significantly lower than its initial concentration. To further examine the influence of the PMAA DP and $[Ca^{2+}]$ on the mode of nanoparticle occlusion, an *in situ* experiment was performed whereby the solution pH, calcium activity and extent of vesicle occlusion were monitored over time (Figure 3a). The solution pH and calcium activity were recorded using a pH meter and a calcium-selective electrode, respectively. The growing crystals were periodically sampled at different time points for SEM studies. The reaction solution pH rapidly increased from ~6 to ~9.5 within the first 30 min and then reached a plateau value at ~9.8 (Figure 3b). The calcium activity also increased rapidly over the same timescale, before subsequently decreasing to a constant value within 3 h. The reaction solution became slightly translucent in the early stages of crystallization, suggesting formation of colloidal amorphous precursor species.^[15] This most

likely accounts for the enhanced calcium activity within the first 30 min. Similar observations were also made for the formation of pure calcite crystals in the absence of any additives (Figure S7). Thus, this initial increase in calcium activity is not caused by the presence of the anionic vesicles but is instead an intrinsic feature of the ammonia diffusion method. Examination of the growing crystals produced at various time points provide useful insights into the vesicle occlusion process, from relatively rare occlusion (t = 30 min) to a few random occlusion events (t = 60–150 min), to somewhat denser occlusion (t = 180 min), and eventually to *uniform* occlusion (t = 210 min). These images suggest that efficient vesicle occlusion does not occur until the latter stages of the crystallization process. This explains why very limited vesicle occlusion is observed in the centre of the calcite crystals, whereas relatively dense *surface-confined* occlusion is achieved at the near-surface of the crystals (see Figure 2). Careful examination of these SEM images revealed the occlusion of vesicle aggregates at, or very near, the crystal surface, see red arrows in Figure 3d (further SEM images are provided in Figure S8). This observation prompted us to investigate the colloidal stability of these anionic vesicles at various $[Ca^{2+}]$. Aqueous electrophoresis studies confirmed that vesicle zeta potentials were significantly less anionic in the presence of $CaCl_2$, suggesting electrostatic binding of Ca^{2+} to the anionic PMAA stabiliser chains (Figure S9). With the exception of the PMAA₂₈-PBzMA₂₀₀ vesicles, dynamic light scattering (DLS) indicated that colloidal stability was retained for $[Ca^{2+}] \leq 5$ mM (Figure S9). Clearly, vesicles bearing shorter PMAA stabilizer chains are less able to tolerate the presence of $CaCl_2$. Moreover, vesicle flocculation was observed at higher

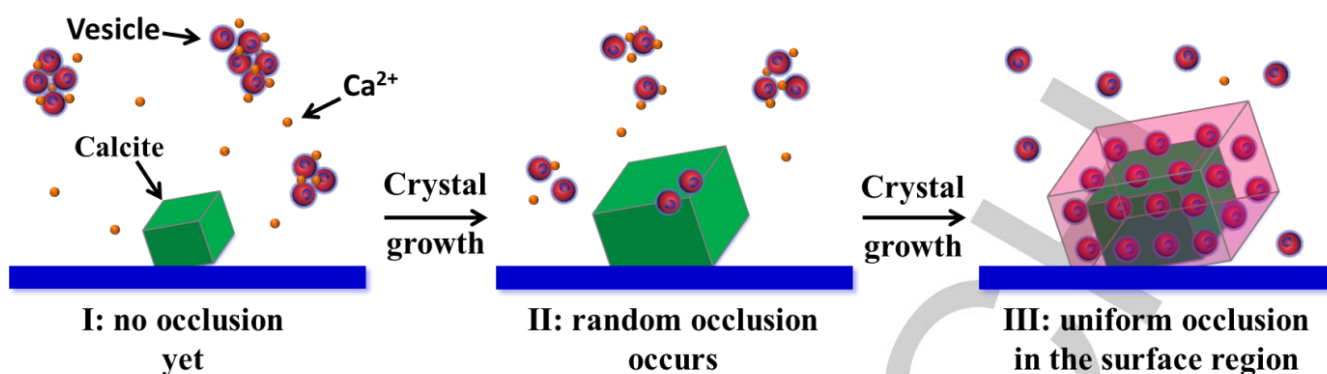


Figure 4. Schematic cartoon depicting the proposed mechanism for the *surface-confined* occlusion of vesicles within calcite crystals. **Stage I**: vesicle flocculation is prevalent at the relatively high initial $[Ca^{2+}]$, thus little or no occlusion occurs. **Stage II**: flocculated vesicles begin to redisperse as Ca^{2+} ions are gradually consumed, leading to a limited amount of random occlusion. **Stage III**: there are now many individual vesicles available for occlusion, although sufficiently long PMAA stabilizer chains are required to ensure efficient occlusion.

$[Ca^{2+}]$ for all four types of vesicles when these aqueous dispersions were allowed to stand at 20 °C for 24 h (**Figure S10**). Vesicle flocculation prevents efficient occlusion within calcite because the flocculated vesicles are much bigger than the individual vesicles. Such aggregates diffuse too slowly to reach the surface of the growing crystals within the required timescale, so their occlusion becomes inefficient. Furthermore, longer PMAA DPs clearly confer greater colloidal stability. This explains why only the PMAA₇₂-PBzMA₂₀₀ vesicles can be uniformly occluded within calcite crystals at $[Ca^{2+}] = 3-4$ mM.

Based on the *in situ* experiments, *surface-confined* vesicle occlusion can be depicted in **Figure 4**. In **Stage I**, the vesicles are flocculated and the resulting vesicle aggregates cannot be occluded within the host crystals. In **Stage II**, the flocculated vesicles begin to redisperse so occlusion of some of the liberated individual vesicles can occur. Finally, in **Stage III**, the $[Ca^{2+}]$ is significantly reduced, so now there are many individual vesicles available for dense, uniform occlusion at the surface of the growing crystals.

Surface-confined occlusion has been observed by various research groups^[2b, 16] and has remained a little-understood phenomenon for more than a decade. In our prior study, we found that using short stabilizer chains led to *surface-confined* occlusion for $[Ca^{2+}] = 1.5$ mM.^[5b] Herein we for the first time show that *surface-confined* occlusion is also closely related to the initial $[Ca^{2+}]$. Moreover, *uniform* occlusion can only be achieved by adjusting both parameters. First, the nanoparticles must be able to bind to the growing crystal surface prior to their engulfment. Indeed, *in situ* atomic force microscopy (AFM) studies revealed that nanoparticles are first preferentially adsorbed onto the step edges before being buried by advancing steps.^[17] Thus, sufficiently long stabilizer chains are essential for *uniform* occlusion because they possess more binding sites and can adopt many more conformations, which facilitates nanoparticle binding at the surface of the growing crystals. Moreover, SAXS studies show that the surface density of stabilizer chains is systematically reduced for PMAA_x-PBzMA₂₀₀ vesicles with increasing x , which also favours vesicle occlusion.^[5c] Nanoparticle occlusion differs significantly from gel incorporation strategies,^[18] whereby nanoparticles become occluded simply via physical entrapment.^[19] Furthermore, in the

present study the initial $[Ca^{2+}]$ indirectly affects the extent of nanoparticle occlusion because it induces flocculation of the PMAA_x-PBzMA₂₀₀ vesicles. Consequently, efficient occlusion cannot be achieved even if the PMAA chains are sufficiently long (**Figure 2e** and **Figure S5**).

Patterned Occlusion of Nanoparticles within Calcite Single Crystals. Achieving spatial control during nanoparticle occlusion is highly desirable but represents a formidable technical challenge.^[20] Recently, Li and co-workers have demonstrated that crystallization within a gel can be used to design the internal structure of potassium dihydrogen phosphate single crystals. By changing the crystallization conditions of growth rate between slow and fast modes or by oscillating the crystallization medium between solutions and gels, patterned internal structures either with or without incorporated gel networks can be obtained.^[20a] Having established a deeper understanding of *surface-confined* occlusion, we sought to control nanoparticle occlusion within the growing calcite crystals to produce patterned regions. For brevity, we denote calcite domains that contain occluded vesicles as **O** and calcite domains containing no occluded vesicles as **N**, respectively. Thus, for example, *surface-confined* occlusion can be denoted as **N/O**. We aimed to prepare either **N/O/N** or **O/N/O** patterned vesicle/calcite structures such that the middle layer of a calcite crystal either contained occluded vesicles or no vesicles. PMAA₇₂-PBzMA₂₀₀ vesicles were selected because the relatively long PMAA DP ensures efficient *uniform* occlusion, as reported above. On the other hand, calcite crystals were prepared using $[Ca^{2+}] = 3$ mM because vesicle flocculation does not occur at this concentration (see **Figure S10**).

Optical micrographs confirm that pure calcite crystals are transparent (**Figure 5a**). A slightly translucent shell owing to *surface-confined* vesicle occlusion was observed for the **N/O** crystals (**Figure 5b**). For **N/O/N** crystals, a transparent outer layer is produced (**Figure 5c**). As expected, complementary observations were made for the **O/N** and **O/N/O** crystals. Because a highly fluorescent comonomer was incorporated within the vesicle membranes, CLSM enables direct visualization of the spatial distribution of vesicles within single calcite crystals (**Figures 5g-r**). Notably, CLSM images provide

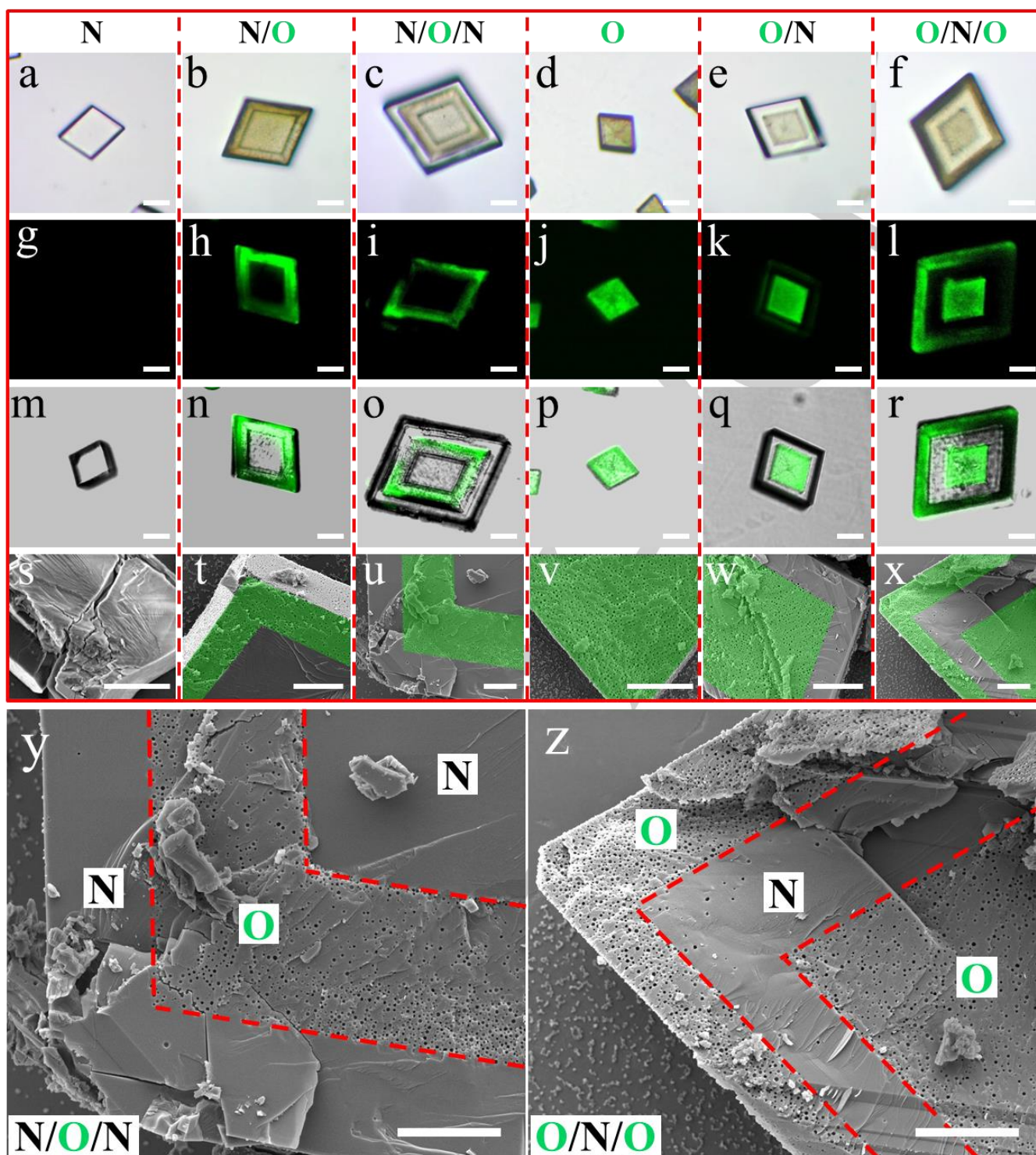


Figure 5. Patterned occlusion of PMAA₇₂-PBzMA₂₀₀ diblock copolymer vesicles within single calcite crystals. (a-f) Optical micrographs; (g-l) confocal laser scanning microscopy (CLSM) images; (m-r) merged CLSM and bright-field optical images; (s-x) SEM images recorded for randomly-fractured calcite crystals revealing patterned vesicle occlusion. The false green color in (t-x) indicates the regions in which vesicle occlusion occurs. (y) and (z) are higher magnification SEM images of (u) and (x), respectively. [N.B. **N** denotes no occlusion while **O** denotes occlusion]. Scale bars for (a-r) and (s-z) indicate 10 μm and 5 μm , respectively.

2D internal cross-sections of such crystals that reveal the expected domain-limited spatial distribution of vesicles (Figures 5h-r). SEM studies of randomly-fractured crystals confirmed well-controlled domains of vesicle occlusion (Figures 5s-x).

More SEM images are provided in supplementary information (Figure S11). Regardless of the type of patterned occlusion, all vesicle/calcite nanocomposite crystals exhibited a rhombohedral morphology, indicating that the crystal growth habit was not

perturbed by vesicle incorporation. Meanwhile, patterned vesicle occlusion does not affect the crystal polymorph, which remains pure calcite as determined by powder XRD studies (**Figure S12**). Remarkably, well-defined boundaries are observed between domains containing occluded vesicles and domains containing no vesicles, as indicated by red dash lines in **Figure 5y** and **Figure 5z**. It is perhaps worth noting that the anionic PMAA stabilizer chains of the occluded vesicles interact strongly with the calcite crystals. Thus random fracture of the nanocomposite crystals leads to rupture of individual vesicles, revealing their lumens as voids.^[5b] Clearly, vesicle occlusion can be manipulated with rather precise spatial control, which suggests a multi-step nanoparticle occlusion strategy for the construction of nanocomposite crystals with patternable internal structures.

Conclusion

The effect of systematically varying the PMAA stabilizer DP and the $[Ca^{2+}]$ on the occlusion of a series of model anionic PMAA_x-PBzMA₂₀₀ vesicles within calcite crystals has been studied. These parameters play important roles in determining whether vesicle occlusion is *uniform* or *surface-confined*. A sufficiently high PMAA DP is required to ensure *uniform* vesicle occlusion while a relatively low $[Ca^{2+}]$ is essential to avoid vesicle aggregation. Furthermore, *in situ* experiments conducted at relatively high $[Ca^{2+}]$ provide important insights regarding surface-confined vesicle occlusion. In summary, our study not only provides important design rules for efficient nanoparticle occlusion, but also enables rational design of new nanocomposite crystals in which the spatial location of guest anionic diblock copolymer vesicles within a calcite host matrix can be precisely controlled.

Acknowledgements

EPSRC (EP/P005241/1) is thanked for post-doctoral support for Y.N., the Leverhulme Trust (RPG-2016-330) is thanked for post-doctoral support for M.J.D. and S.P.A. acknowledges an EPSRC Established Career Particle Technology Fellowship (EP/R003009/1). We thank the beamline staff of I22, Diamond Light Source, for their assistance in SAXS data acquisition.

Keywords: Polymerization-induced self-assembly (PISA) • block copolymer vesicles • spatially-controlled occlusion • patterned structure • calcite (CaCO₃)

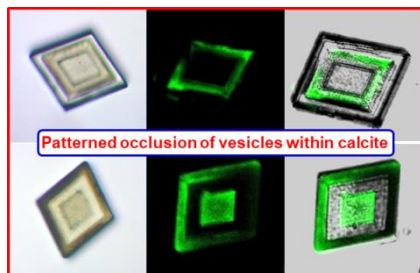
- [1] Y. Ning, S. P. Armes, *Acc. Chem. Res.* **2020**, *53*, 1176-1186.
- [2] a) R. Muñoz - Espí, Y. Qi, I. Lieberwirth, C. M. Gomez, G. Wegner, *Chem. Eur. J.* **2006**, *12*, 118-129; b) Y. Y. Kim, L. Ribeiro, F. Maillot, O. Ward, S. J. Eichhorn, F. C. Meldrum, *Adv. Mater.* **2010**, *22*, 2082-2086; c) G. Lu, S. Li, Z. Guo, O. K. Farha, B. G. Hauser, X. Qi, Y. Wang, X. Wang, S. Han, X. Liu, *Nat. Chem.* **2012**, *4*, 310.
- [3] a) Y.-Y. Kim, K. Ganesan, P. Yang, A. N. Kulak, S. Borukhin, S. Pechook, L. Ribeiro, R. Kröger, S. J. Eichhorn, S. P. Armes, B. Pokroy, F. C. Meldrum, *Nat. Mater.* **2011**, *10*, 890-896; b) Y. Y. Kim, M. Semsarilar, J. D. Carloni, K. R. Cho, A. N. Kulak, I. Polishchuk, C. T. Hendley IV, P. J. Smeets, L. A. Fielding, B. Pokroy, *Adv. Funct. Mater.* **2016**, *26*, 1382-1392.
- [4] Y. Ning, L. A. Fielding, K. E. Doncom, N. J. Penfold, A. N. Kulak, H. Matsuoka, S. P. Armes, *ACS Macro Lett.* **2016**, *5*, 311-315.
- [5] a) Y. Ning, L. Han, M. J. Derry, F. C. Meldrum, S. P. Armes, *J. Am. Chem. Soc.* **2019**, *141*, 2557-2567; b) Y. Ning, L. Han, M. Douverne, N. J. W. Penfold, M. J. Derry, F. C. Meldrum, S. P. Armes, *J. Am. Chem. Soc.* **2019**, *141*, 2481-2489; c) Y. Ning, L. A. Fielding, L. P. D. Ratcliffe, Y.-W. Wang, F. C. Meldrum, S. P. Armes, *J. Am. Chem. Soc.* **2016**, *138*, 11734-11742; d) A. N. Kulak, M. Semsarilar, Y.-Y. Kim, J. Ihli, L. A. Fielding, O. Cespedes, S. P. Armes, F. C. Meldrum, *Chem. Sci.* **2014**, *5*, 738-743; e) M. Douverne, Y. Ning, A. Tatani, F. C. Meldrum, S. P. Armes, *Angew. Chem. Int. Ed.* **2019**, *58*, 8692-8697; f) Y. Ning, L. Fielding, T. Andrews, D. Gowney, S. Armes, *Nanoscale* **2015**, *7*, 6691-6702; g) G. Magnabosco, I. Polishchuk, F. Palomba, E. Rampazzo, L. Prodi, J. Aizenberg, B. Pokroy, G. Falini, *Cryst. Growth & Des.* **2019**, *19*, 4429-4435; h) Y. Ning, F. C. Meldrum, S. P. Armes, *Chem. Sci.* **2019**, *10*, 8964-8972.
- [6] a) N. J. Warren, S. P. Armes, *J. Am. Chem. Soc.* **2014**, *136*, 10174-10185; b) J. Yeow, C. Boyer, *Adv. Sci.* **2017**, *4*, 1700137; c) F. D'Agosto, J. Rieger, M. Lansalot, *Angew. Chem. Int. Ed.*, doi:10.1002/anie.201911758.
- [7] a) J. Chiefari, Y. Chong, F. Ercole, J. Krstina, J. Jeffery, T. P. Le, R. T. Mayadunne, G. F. Meijs, C. L. Moad, G. Moad, *Macromolecules* **1998**, *31*, 5559-5562; b) A. B. Lowe, C. L. McCormick, *Prog. Polym. Sci.* **2007**, *32*, 283-351.
- [8] a) X. Wang, Z. An, *Macromol. Rapid Commun.* **2019**, *40*, 1800325; b) Y. Ding, M. Cai, Z. Cui, L. Huang, L. Wang, X. Lu, Y. Cai, *Angew. Chem. Int. Ed.* **2018**, *57*, 1053-1056; c) J. C. Foster, S. Varlas, B. Couturaud, J. R. Jones, R. Keogh, R. T. Mathers, R. K. O'Reilly, *Angew. Chem.* **2018**, *130*, 15959-15963; d) S.-I. Chen, P.-f. Shi, W.-q. Zhang, *Chin. J. Polym. Sci.* **2017**, *35*, 455-479; e) R. Deng, M. J. Derry, C. J. Mable, Y. Ning, S. P. Armes, *J. Am. Chem. Soc.* **2017**, *139*, 7616-7623.
- [9] a) G. Mellot, J. M. Guigner, L. Bouteiller, F. Stoffelbach, J. Rieger, *Angew. Chem.* **2019**, *131*, 3205-3209; b) J. Tan, H. Sun, M. Yu, B. S. Sumerlin, L. Zhang, *ACS Macro Lett.* **2015**, *4*, 1249-1253; c) W.-M. Wan, C.-Y. Hong, C.-Y. Pan, *Chem. Commun.* **2009**, 5883-5885; d) P. Yang, Y. Ning, T. J. Neal, E. R. Jones, B. R. Parker, S. P. Armes, *Chem. Sci.* **2019**, *10*, 4200-4208; e) M. Huo, M. Zeng, D. Li, L. Liu, Y. Wei, J. Yuan, *Macromolecules* **2017**, *50*, 8212-8220; f) F. Lv, Z. An, P. Wu, *Nat. Commun.* **2019**, *10*, 1397.
- [10] J. Bang, S. Jain, Z. Li, T. P. Lodge, J. S. Pedersen, E. Kesselman, Y. Talmon, *Macromolecules* **2006**, *39*, 1199-1208.
- [11] Y. Ning, D. J. Whitaker, C. J. Mable, M. J. Derry, N. J. Penfold, A. N. Kulak, D. C. Green, F. C. Meldrum, S. P. Armes, *Chem. Sci.* **2018**, *9*, 8396-8401.
- [12] M. J. Derry, L. A. Fielding, N. J. Warren, C. J. Mable, A. J. Smith, O. O. Mykhaylyk, S. P. Armes, *Chem. Sci.* **2016**, *7*, 5078-5090.
- [13] G. Battaglia, A. J. Ryan, *J. Am. Chem. Soc.* **2005**, *127*, 8757-8764.
- [14] J. Ihli, P. Bots, A. Kulak, L. G. Benning, F. C. Meldrum, *Adv. Funct. Mater.* **2013**, *23*, 1965-1973.
- [15] Y. Y. Kim, C. L. Freeman, X. Gong, M. A. Levenstein, Y. Wang, A. Kulak, C. Anduix - Canto, P. A. Lee, S. Li, L. Chen, *Angew. Chem. Int. Ed.* **2017**, *56*, 11885-11890.
- [16] a) C. Lu, L. Qi, H. Cong, X. Wang, J. Yang, L. Yang, D. Zhang, J. Ma, W. Cao, *Chem. Mater.* **2005**, *17*, 5218-5224; b) A. Hanisch, P. Yang, A. N. Kulak, L. A. Fielding, F. C. Meldrum, S. P. Armes, *Macromolecules* **2015**, *49*, 192-204.
- [17] a) K. Rae Cho, Y.-Y. Kim, P. Yang, W. Cai, H. Pan, A. N. Kulak, J. L. Lau, P. Kulshreshtha, S. P. Armes, F. C. Meldrum, J. J. De Yoreo, *Nat. Commun.* **2016**, *7*, 10187; b) C. T. Hendley, L. A. Fielding, E. R. Jones, A. J. Ryan, S. P. Armes, L. A. Estroff, *J. Am. Chem. Soc.* **2018**, *140*, 7936-7945; c) J. Chi, W. Zhang, L. Wang, C. V. Putnis, *Environ. Sci. Technol.* **2019**, *53*, 8097-8104; d) H. H. Teng, P. M. Dove, C. A. Orme, J. J. De Yoreo, *Science* **1998**, *282*, 724-727.
- [18] H. Li, H. L. Xin, D. A. Muller, L. A. Estroff, *Science* **2009**, *326*, 1244-1247.
- [19] a) Y. Liu, W. Yuan, Y. Shi, X. Chen, Y. Wang, H. Chen, H. Li, *Angew. Chem. Int. Ed.* **2014**, *53*, 4127-4131; b) Y. Liu, H. Zang, L. Wang, W. Fu, W. Yuan, J. Wu, X. Jin, J. Han, C. Wu, Y. Wang, H. Xin, H. Chen, H. Li, *Chem. Mater.* **2016**, *28*, 7537-7543.
- [20] a) X. Jin, L. Chen, Y. Liu, T. Ye, C. Hu, J. Ren, H. Chen, H. Li, *J. Phys. Chem. C* **2019**, *123*, 13147-13153; b) D. C. Green, J. Ihli, P. D.

Thornton, M. A. Holden, B. Marzec, Y.-Y. Kim, A. N. Kulak, M. A. Levenstein, C. Tang, C. Lynch, S. E. D. Webb, C. J. Tynan, F. C. Meldrum, *Nat. Commun.* **2016**, *7*, 13524; c) J. Aizenberg, J. Hanson, T. F. Koetzle, S. Weiner, L. Addadi, *J. Am. Chem. Soc.* **1997**, *119*, 881-886; d) A. G. Shtukenberg, M. D. Ward, B. Kahr, *Chem. Rev.* **2017**, *117*, 14042-14090; e) R. A. Metzler, G. A. Tribello, M. Parrinello, P. U. P. A. Gilbert, *J. Am. Chem. Soc.* **2010**, *132*, 11585-11591; f) Y. Ning, L. A. Fielding, J. Nutter, A. N. Kulak, F. C. Meldrum, S. P. Armes, *Angew. Chem. Int. Ed.* **2019**, *58*, 4302-4307.

WILEY-VCH

Accepted Manuscript

Entry for the Table of Contents



We show that both surface chemistry and $[\text{Ca}^{2+}]$ concentration play critical roles in dictating the precise spatial occlusion of the guest nanoparticles within calcite crystals. This new insight enables the rational design of patterned nanocomposite crystals via a multi-step occlusion strategy.